MNRAS **000**, 1–5 (2016) Preprint 28 October 2016 Compiled using MNRAS LATEX style file v3.0

RRM observations of the short burst GRB160410A located at z = 1.717. Chemical conditions and kinematics.⋆

Jonatan Selsing,[1]† Everyone in some order,[1]
[1]*Dark Cosmology Centre, Niels Bohr Institute, University of Copenhagen, Juliane Maries Vej 30, 2100 Copenhagen, Denmark.*

Accepted XXX. Received YYY; in original form ZZZ

ABSTRACT
GRB160410A was observed using the Rapid Response Mode (RMM) of X-shooter, in which observations began 8.2 minutes after the *Swift* trigger. Due to the short delay between the trigger and observations, an unprecedented quality of data was obtained allowing a unambiguous determination of the highest redshift short GRB ever observed at z=1.717. This allows a detailed investigation of the chemical conditions of sight-line towards the GRB in which a very low-ionization medium is seen local to the burst. This agrees well with the longer delay-time for short bursts due to the neutron star - neutron star merger timescale being longer than the ..

Key words: keyword1 – keyword2 – keyword3

1 INTRODUCTION

For a brief moment, gamma-ray bursts (GRBs) outshine every other source in the known universe. With durations ranging from milliseconds to thousands of second, they are broadly categorized in two groups, long- and short GRBs (ref). The distinction of GRBs into two groups is based on a clear bi-modality in both duration and spectral hardness with the short bursts having harder radiation (ref). The short bursts are usually associated with the merger of two neutron stars (NS), which if in a binary system will experience gravitational decay causing a in spiral of the orbit, finally leading to the coalescence of the two compact objects. Several lines of evidence in support of this model include the detection of a "kilo-nova" in conjunction with the short GRB 130603B (Tanvir et al. 2013; Berger et al. 2013). Additionally, the detection of gravitational waves from what seems to be a BH-BH merger confirms the occurrence of the type of system that could could give rise to a short GRB (LVC16a et al. 2016).

2 OBSERVATIONS

2.1 *Swift* detection

The Burst Alert Telescope (BAT) onboard the *Swift* space telescope (Gehrels et al. 2004) triggered on a source on the 10th of April, 2016 at 05:09:48.05 UT.

Norris et al. (2011)

2.2 Photometric host-search

2.3 X-shooter observations

The robotic rapid-response mode (RMM) was automatically triggered by *Swift* and observations of the afterglow of GRB160410A began with X-shooter (Vernet et al. 2011) at 05:18:08.00 UT, 8.6 minutes after the *Swift* trigger. The observations was carried out under ESO programme 097.A-0036(A). X-shooter is a single-slit, cross-dispersion echelle spectrograph mounted on UT2 (Kueyen), at the European Southern Observatory (ESO) Very Large Telescope (VLT). Simultaneous coverage of the spectral range 3100 - 24800Å distributed among three spectral arms (UVB: 3100 - 5500 Å, VIS: 5500 - 10150 Å and NIR: 10150 - 24800 Å) allows for the concurrent detection of the Lyα-absorption and search for potential emission lines visible in the near-infrared, important for confirming the redshifts of the potential host and/or intervening systems. The observations of GRB160410A consist of 3 exposures of 600 s each in a dithering pattern ABB taken just before the twilight until the telescope reached the hardware limit of 20 deg in altitude. The seeing conditions were excellent at zenith and decent on target ($\sim 0\farcs9$). The transparency conditions were clear. Because the target was just above the horizon, the airmass was ~ 2.4 and consequently due the malfunctioning ADC, the spectral trace changes spatial position on the slit as a function of wavelength. We model this in the spectral extraction. The spectra are reduced using the ESO/X-shooter pipeline v. 2.6.8 (Modigliani et al. 2010) and organized using Reflex (Freudling et al. 2013). An initial sky-subtraction is

⋆ Based on observations made with telescopes at the European Southern Observatory at La Silla/Paranal, Chile under program 097.A-0036(A).
† E-mail: jselsing@dark-cosmology.dk

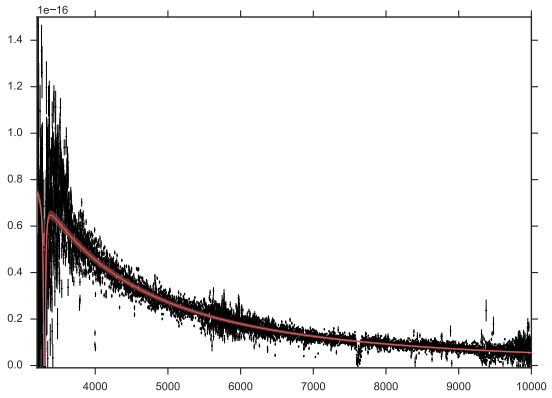

Figure 1. The voigt-profile fit to the Lyα-absorption. The black dots with errorbars is the data and associated errors for the spectrum, binned by 10 pixels. The fit is performed on the un-binned spectrum. The red line is the fit obtained using the median value of the posterior distribution of each of the fit parameters with the red shaded area representing the 1-σ width of the distribution.

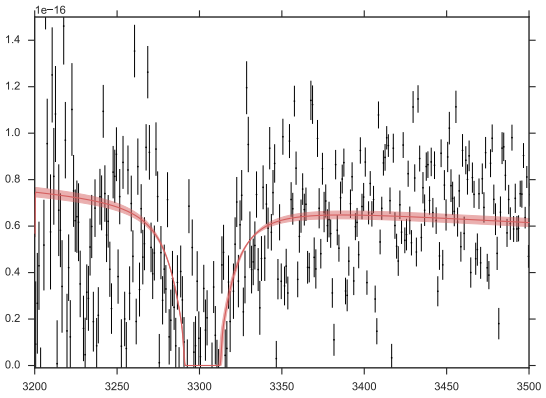

Figure 2. The voigt-profile fit to the Lyα-absorption. The black dots with errorbars is the data and associated errors for the spectrum, binned by 10 pixels. The fit is performed on the un-binned spectrum. The red line is the fit obtained using the median value of the posterior distribution of each of the fit parameters with the red shaded area representing the 1-σ width of the distribution.

performed on the un-rectified image The spectral response function is generated using observations of a spectrophotometric standard-star (Vernet et al. 2009; Hamuy et al. 1994), where the flux of the stardard star is optimally extracted because we also optimally extract GRB160410A.

3 CHEMICAL ABUNDANCES AND KINEMATICS

Using the absorption lines detected against the bright continuum, it is possible to infer the conditions present along the line-of-sight towards the GRB. Specifically, by measuring the hydrogen column density and various metals, it is possible to put constraints on the metallicity.

3.1 Hydrogen column density

From the detection of absorption by Lyα at the redshift of the burst, we can infer the hydrogen column density present locally a the position of the burst.

3.2 Line-analysis

3.2.1 Kinematic analysis

3.2.2 Line-strength analysis

I did some initial numbers on 160410A, see the table below and the attached figure. I still need to refine this a bit and calculate some further detection limits. The lines are quite weak, as compared to the sample that I used in my paper. I get a LSP of -1.57+/-0.87. This means that the spectrum has features that are stronger than only 1.6 percent of the sample (or weaker than 98.4 percent). I attach a table with some line detections. We have no detection of MgII because it falls in the telluric A-band, which is also very strong at the airmass that we observed.

I'm very surprised that the Keck people see Si II, O I,

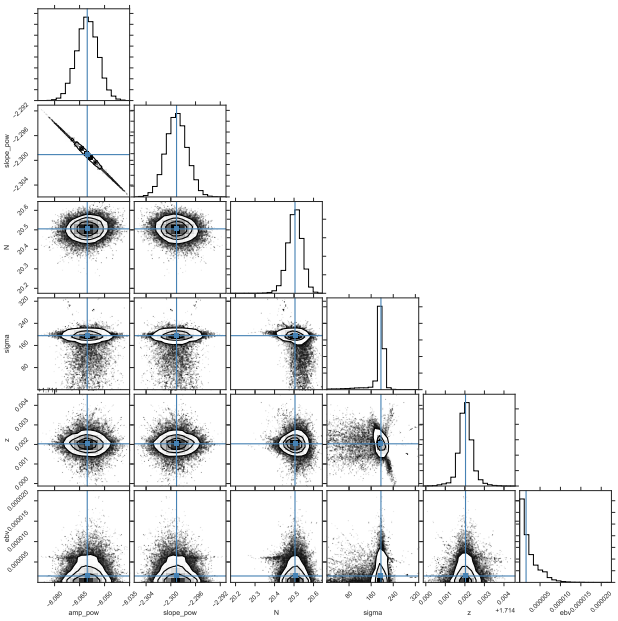

Figure 3. Cornerplot of the fitted parameters showing the posterior distribution of each parameter along with potential correlations. As can be seen the continuum slope and amplitude are highly correlated, as expected. The weak dependence on the thermal line-broadening is visible from the wide range of acceptable values. We give the most likely parameter values as well as their credible intervals in 3.1

C IV and Mg II in their single 600s spectrum. Maybe with a good telluric correction and lower airmass (they observed at an airmass of 1.05) they can see MgII (there are also minima at the right locations in our spectra), but I get a 3-sigma limit of ~0.5 Å for CIV (0.18 Å in rest frame for each of the lines), and there is really no hint of anything there, nothing. SiII is there and OI could show something at very

Table 1. Line-strengths inferred.

Wavelength[(a)] (Å)	Range (Å)	EW (Å)	Feature	z	H I column density log(N/cm^2)
					$21.3^{+0.31}_{-0.29}$

[(a)] Blalba .

low significance, but not CIV. An then they don't see any FeII or AlII that we do see.

Either they have invented some lines and ignored others, or the spectrum of this GRB changed a lot during the first hour and a half. I wonder, in that case if there is any variation between our spectra.

Furthermore, we see no SiIV, which together with the detection of SiII and the lack of CIV points towards a low ionisation environment. There is no AlIII either in spite of the AlII, so more to that argument. Line variability may not be a crazy thought, as we observed really soon, but its still weird. Maybe someone could find out more about the Keck spectrum? Perhaps they are willing to contribute to whatever paper comes out of this by providing it (given that what they claim is real!).

In any case this is a peculiar spectrum with a low column density and low ionisation environment. There are also no hints of fine structure lines in spite of the prompt spectrum. I don't know if this means that it is a short GRB, but it is for sure weird.

4 ENVIRONMENTAL CENSUS

5 DISCUSSION

6 CONCLUSIONS

ACKNOWLEDGEMENTS

The Acknowledgements section is not numbered. Here you can thank helpful colleagues, acknowledge funding agencies, telescopes and facilities used etc. Try to keep it short.

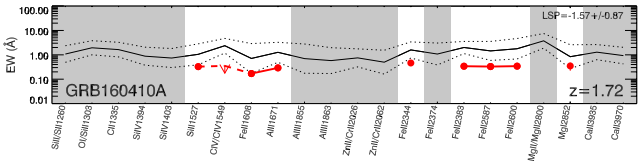

Figure 4. Schematic illustration of the thermal evaporation. *TODO* : Placeholder

REFERENCES

Abrarov S. M., Quine B. M., 2015a, J. Math. Res., 7, 44
Abrarov S. M., Quine B. M., 2015b, J. Math. Res., 7, 163
Benner D., Rinsland C. P., Devi V., Smith M. A. H., Atkins D., 1995, J. Quant. Spectrosc. Radiat. Transf., 53, 705
Berger E., Fong W., Chornock R., 2013, Astrophys. J., 774, L23
Fitzpatrick E. L., Massa D., 2007, Astrophys. J., 663, 320
Freudling W., Romaniello M., Bramich D. M., Ballester P., Forchi V., García-Dabló C. E., Moehler S., Neeser M. J., 2013, Astron. Astrophys., 559, A96
Gehrels N., et al., 2004, Astrophys. J., 611, 1005
Gordon K. D., Clayton G. C., Misselt K. A., Landolt A. U., Wolff M. J., 2003, Astrophys. J., 594, 279
Hamuy M., Suntzeff N. B., Heathcote S. R., Walker A. R., Gigoux P., Phillips M. M., 1994, Publ. Astron. Soc. Pacific, 106, 566
Hogg D. W., Bovy J., Lang D., 2010
Japelj J., et al., 2015, Astron. Astrophys., 579, A74
Jones E., Oliphant T., Peterson P., 2001, SciPy: Open source scientific tools for Python, http://www.scipy.org/
Kumar P., Zhang B., 2015, Phys. Rep., 561, 1
LVC16a et al., 2016, Phys. Rev. Lett., 116, 061102
Letchworth K. L., Benner D. C., 2007, J. Quant. Spectrosc. Radiat. Transf., 107, 173
Modigliani A., et al., 2010, SPIE Astron. Telesc. + Instrum., 7737, 773728
Norris J. P., Gehrels N., Scargle J. D., 2011, Astrophys. J., 735, 23
Pagnini G., Mainardi F., 2010, J. Comput. Appl. Math., 233, 1590
Piran T., 2004, Rev. Mod. Phys., 76
Tanvir N. R., Levan a. J., Fruchter a. S., Hjorth J., Hounsell R. a., Wiersema K., Tunnicliffe R. L., 2013, Nature, 500, 547
Tepper García T., 2006, Mon. Not. R. Astron. Soc., 369, 2025
Vernet J., et al., 2009, Proc. Int. Astron. Union, 5, 535
Vernet J., et al., 2011, Astron. Astrophys., 536, A105

Table 2. Line-strengths inferred.

Wavelength[(a)] (Å)	Range (Å)	EW (Å)	Feature	z
3406.7	3404.3 - 3408.3	2.148± 0.601	SII 1253.520	1.71771 (1.71760)
			SiIV 1393.8	1.44425 (1.44450)
3784.6	3784.0 - 3785.6	0.916± 0.188	CIV 1548.200	1.44449 (1.44450)
3790.6	3789.2 - 3791.2	0.918± 0.212	CIV 1550.770	1.44430 (1.44450)
3996.5	3995.2 - 3998.4	1.548± 0.199	CIV 1548.200	1.58136 (1.58150)
4003.2	4002.0 - 4004.0	1.260± 0.165	CIV 1550.770	1.58145 (1.58150)
4084.1	4083.3 - 4084.9	0.339± 0.137	AlII 1670.790	1.44443 (1.44450)
4150.1	4148.1 - 4152.5	0.890± 0.176	SiII 1526.710	1.71830 (1.71760)
			FeII 1608.5	1.58016 (1.58150)
4371.6	4370.5 - 4372.5	0.463± 0.111	FeII 1608.450	1.71789 (1.71760)
4540.8	4539.3 - 4542.1	0.792± 0.179	AlII 1670.790	1.71775 (1.71760)
5732.4	5730.8 - 5734.8	0.853± 0.377	FeII 2345.000	1.44454 (1.44450)
6371.1	6369.7 - 6372.9	1.259± 0.262	FeII 2344.210	1.71782 (1.71760)
			FeII 2345.0	1.71691 (1.71760)
6475.5	6474.1 - 6476.1	0.927± 0.172	FeII 2382.770	1.71764 (1.71760)
7029.5	7028.2 - 7030.6	0.898± 0.158	FeII 2586.650	1.71762 (1.71760)
7066.5	7065.4 - 7069.0	0.932± 0.183	FeII 2600.170	1.71772 (1.71760)
7753.7	7752.4 - 7754.8	0.951± 0.346	MgI 2852.960	1.71776 (1.71760)
9619.0	9616.7 - 9620.3	0.996± 0.345	CaII 3934.780	1.44461 (1.44450)

[(a)] Blalba .

APPENDIX A: CONTINUUM MODEL

The optical- and near-infrared continuum of GRB afterglows can be described by a single power law, owing to the continuum generation by syncrotron radiation in the forward shock of the ejected material (Piran 2004; Kumar & Zhang 2015),

$$S_\lambda = S_0 \lambda^{-\beta}, \tag{A1}$$

where S_0 is an arbitrary scaling factor for the flux density and β is the power-law slope, both free parameters. Additionally, light is attenuated by the presence dust particles which preferentially absorbs shorter wavelength photons, where the detailed dependence is set by the composition of the dust grains. Extinction curves have been parametrized in terms of various shape parameters. We use the parametrization by Fitzpatrick & Massa (2007) with the values of SMC-like dust (Gordon et al. 2003) for our initial guess, based on the prevalence of SMC-like dust in GRB host galaxies (Japelj et al. 2015),

$$S_\lambda = S^*_\lambda 10^{-0.4E(B-V)[k(\lambda-V)+R_V]}, \tag{A2}$$

where S^*_λ is again the unreddened flux value, $E(B-V)$ is the color excess, R_V is the total to selective extinction, meaning how many mangitudes absorption per color excess, and $k(\lambda - V)$ is the wavelength dependent extinction curve,

$$k(\lambda - V) \begin{cases} c_1 + c_2 x + c3 \frac{x^2}{(x-x_0)^2+x^2\gamma^2}, & x \leq c_5, \\ c_1 + c_2 x + c3 \frac{x^2}{(x-x_0)^2+x^2\gamma^2} + c_4(x-c_5)^2, & x > c_5, \end{cases} \tag{A3}$$

where $x \equiv \lambda^{-1}$ and the rest, c_1 through c_5 are shape parameters for the extinction curve (Fitzpatrick & Massa 2007).

The continuum level emission will therefore by the product of the intrinsic power-law shape, absorbed by some extinction curve.

APPENDIX B: LYMAN-α COLUMN DENSITY

The background continuum experiences absorption by intervening material, the strength of which depends on specifics about the absorbing material as well as the abundance of it. The change in flux observed as the light travels through a cloud of material is given by the solution to the equation of radiative transfer without emissivity

$$S_\lambda = S^*_\lambda \, e^{-\sigma_\lambda N_j}, \tag{B1}$$

where S^*_λ is the incident flux, S_λ is the resulting flux, σ_λ is the wavelength dependent, transition-specific cross section and N_j is the column density of the absorbable species in state j (the state number-density n_j intergrated over the entire line of sight, ds). Therefore the strength of absorption is directly related to the column of material that we see through. The exponent equals the optical depth, τ_λ, and gives the probability that a photon with a given wavelength is absorbed. The wavelength-dependent atomic absorbtion cross-section, σ_λ, is composed of two parts; the integrated transition cross-section, $\sigma_{jk} = \int_0^\infty \sigma_\lambda d\lambda$ for the transition from state j to state k and the line shape profile ϕ_λ, which reflects the probability of a photon being absorbed at a given wavelength. σ_{jk} can be calculated from considering the Hamiltonian of the photon - atom interaction and when disregarding stimulated emission and it is set by the oscillator strength of the transition, f_{jk}, the elementary charge, e, and the mass of the electron, m_e, - quantities independent

of the environments in which the absorption takes place,

$$\sigma_{jk} = \int_0^\infty \sigma_\lambda d\lambda = \frac{\pi e^2}{m_e c} f_{jk}. \tag{B2}$$

Several processes broaden the probability distribution of absorption and consists of classes, inherently either Lorentzian of Gaussian in shape. The sum of broadening mechanisms can be parametrized by the convolution of the Gaussian with the Lorentzian profile, called the Voigt profile ,$V(\lambda, \sigma, \gamma)$. This profile is specified by the respective widths, σ for the Gaussian and γ for the Lorentzian. At the densities considered for the absorption, the natural line broadening mechanism dominates the Lorentzian width and is given by $\gamma = \sum_{j<k} A_{jk}$, and is thus specified by specifics of the transition, leaving only the Gaussian width and the column density to control the absorption-probability. The absorption signature in a continuum due to a single atomic transition can thusly be parametrized as

$$S_\lambda = S^*_\lambda \; e^{-\frac{\pi e^2}{m_e c} f_{jk} \lambda_{jk} V(\lambda,\sigma,\gamma) N_j}, \tag{B3}$$

where only N_j, and σ are free parameters, the rest are specified by the continuum level, S^*_λ, transition (Tepper García 2006).

APPENDIX C: LIKELIHOOD MODEL

We are interested in exploring the underlying physical parameters that we believe generate our data. In the case of absorption lines, we believe that the column density of the material and the turbulent motion of the gas are the scalar variables that are sufficient to accurately generate the line shape, see B. What we want to quantify is the range of parameter values that, within measurement uncertainties, contain the true physical parameter value. For each spectral point we have for the GRB afterglow, we believe there is an underlying model that can generate that specific data point, $f(\lambda_i, \theta)$, where θ is the parameters of the model. Following Hogg et al. (2010), we state a *generative model* for the data, where each data point, $S_{i\lambda}$, and associated error, $\delta S_{i\lambda}$, is seen as a normally distributed probability distribution function with the data value being the mean and the y-error, the 1-σ width. If we wanted to repeat the measurement, we could resample the entire spectrum where for each point, the value is drawn from the probability distribution function defined by the current measurements. Using our generative model, each data point $(\lambda, S_{i\lambda}, \delta S_{i\lambda})$ has a conditional probability

$$p(\lambda_i, I(\lambda)_i | \theta, \delta S_{i\lambda}) = \frac{1}{\sqrt{2\pi \delta S^2_{i\lambda}}} exp\left(-\frac{[S_{i\lambda} - f(\lambda, \theta)]^2}{2\delta S^2_{i\lambda}}\right), \tag{C1}$$

where $f(\lambda, \theta)$ is the physical underlying model for the data

$$f(\lambda, \theta) = S_0 \lambda^{-\beta} \prod_{t=i}^{k} e^{-\frac{\pi e^2}{m_e c} f_t \lambda_t V(\lambda,\sigma,\gamma) N_t} 10^{-0.4E(B-V)[k(\lambda-V)+R_V]}. \tag{C2}$$

Here the product is over all absorption lines included in the fit, one component for each transition modeled marked by the subscript, t, up to any value k.

APPENDIX D: THE COMPLEX ERROR FUNCTION AND THE VOIGT PROFILE

As part of the evaluation of the likelihood function we need to evaluate the Voigt-profile. The Voigt profile, which is the convolution of the Gaussian and Lorentzian profiles, can, centered at zero, be written as (Pagnini & Mainardi 2010)

$$\begin{aligned} V(\lambda, \sigma, \gamma) &= G(\lambda, \sigma) \otimes L(\lambda, \gamma) \\ &= \int_{-\infty}^{\infty} G(\xi, \sigma) L(\lambda - \xi, \gamma) d\xi \\ &= \int_{-\infty}^{\infty} \frac{1}{\sqrt{2\pi}\sigma} e^{-\left(\frac{\xi}{\sqrt{2}\sigma}\right)^2} \frac{1}{\gamma\pi} \frac{\gamma^2}{(\lambda - \xi)^2 + \gamma^2} d\xi \\ &= \frac{\gamma}{\sqrt{2}\sigma} \frac{1}{\pi^{3/2}} \int_{-\infty}^{\infty} \frac{e^{-\left(\frac{\xi}{\sqrt{2}\sigma}\right)^2}}{(\lambda - \xi)^2 + \gamma^2}. \end{aligned} \tag{D1}$$

We can by making the following substitution, $\xi = \sqrt{2}\sigma$ and $d\xi = \sqrt{2}\sigma dt$, write it as

$$\begin{aligned} V(\lambda, \sigma, \gamma) &= \frac{\sqrt{2}\sigma}{\sqrt{\pi}} \frac{\frac{\gamma}{\sqrt{2}\sigma}}{\pi} \int_{-\infty}^{\infty} \frac{e^{-t^2}}{(\lambda - \sqrt{2}\sigma t)^2 + \gamma^2} dt \\ &= \frac{1}{\sqrt{2\pi}\sigma} \frac{\frac{\gamma}{\sqrt{2}\sigma}}{\pi} \int_{-\infty}^{\infty} \frac{e^{-t^2}}{\left(\frac{\lambda}{\sqrt{2}\sigma} - t\right)^2 + \left(\frac{\gamma}{\sqrt{2}\sigma}\right)^2} dt. \end{aligned} \tag{D2}$$

This form of the convolution is closely related to the complex probability function (Letchworth & Benner 2007; Abrarov & Quine 2015a),

$$W(z) = \frac{i}{\pi} \int_{-\infty}^{\infty} \frac{e^{-t^2}}{z - t} \tag{D3}$$

for any complex argument, $z = x + iy$. The complex probability function can be expressed as a sum of a real an imaginary part (Benner et al. 1995; Abrarov & Quine 2015b),

$$\begin{aligned} W(x, y) &= K(x, y) + iL(x, y) \\ &= \frac{y}{\pi} \int_{-\infty}^{\infty} \frac{e^{-t^2}}{(x - t)^2 + y^2} dt + \frac{i}{\pi} \int_{-\infty}^{\infty} \frac{(x - t) e^{-t^2}}{(x - t)^2 + y^2} dt, \end{aligned} \tag{D4}$$

where is the real part, $\texttt{Re}[W(x, y)] = \sqrt{2\pi}\sigma V(\lambda, \sigma, \gamma)$ if $x = \frac{\lambda}{\sqrt{2}\sigma}$ and $y = \frac{\gamma}{\sqrt{2}\sigma}$, which can be obtained by using the complex argument, $z = \frac{\lambda + i\gamma}{\sqrt{2}\sigma}$, in the complex probability function. If $\texttt{Im}[z] \geq 0$, which is always guaranteed for the width of a spectral profile, the complex probability function equals the complex error function. The complex error function has numerous, fast, numerical approximations where in this work we use the `scipy.special.wofz` (Jones et al. 2001) implementation.

This paper has been typeset from a TEX/LATEX file prepared by the author.